Biophysical Journal, Volume *110*

Supplemental Information

Molecular Basis of S100A1 Activation at Saturating and Subsaturating Calcium Concentrations

Caitlin E. Scott and Peter M. Kekenes-Huskey

1 Supplement

1.1 Methods

1.1.1 Molecular dynamics setup

In addition to the general setup protocol for the molecular simulations explained in the Methods section, we provide the following configuration details. Covalent bonds containing hydrogen atoms were constrained by the SHAKE algorithm, thus justifying the use of a 2 fs time step for all trials (1, 2). Periodic boundary conditions (PBC) were applied during all minimization and dynamics steps. Minimization consisted of 1000 steps with the protein held fixed with restraints of 500.0 kcal/(mol $\AA^2$) using steepest descent and conjugate gradient optimization methods. This step was followed by 5000 steps of minimization, using the same scheme except with all the atoms movable. For the molecular dynamics runs, the Berendsen thermostat and barostat (for constant pressure simulations) were used (3), while non-bonding interactions were calculated using the particle mesh Ewald (PME) method (4) with a cut-off of 10 Å. The first equilibration step entailed heating the waters and counter ions with the protein fixed via the AMBER belly command from 0 to 300 K for the first 0.08 ns before being held at a constant temperature of 300 K for the final 0.02 ns of the MD constant volume simulations. This simulation was followed by heating the entire system with all atoms movable from 0 to 300 K for the first 0.4 ns before running at a constant 300 K for the remaining 0.1 ns of the 0.5 ns NVT MD. The final equilibration step was a 1 ns MD NPT run at 300 K and 1 bar with everything movable with a pressure relaxation time of 2.0 ps. For the production runs, the atoms' velocities were randomly initialized, and the simulations were conducted with a 2 fs time step at a constant temperature of 300 K and a constant pressure of 1.0 bar with a 2.0 ps pressure relaxation time.

Minimization and early steps of equilibration were conducted on 3.60 GHz Intel Core i7-3820 central processing units (CPUs). The production simulations were run on graphical processing units (GPUs) GeForce GTX 780 with driver

version: 346.59 or on the 2.6 GHz Intel EM64T Xeon E5 CPUs on the XSEDE supercomputer SDSU Gordon Compute cluster.

1.2 Molecular mechanics electrostatic energy

For comparison and validation with our calculated electrostatic score (discussed above), we calculated the molecular mechanics electrostatic energy from the binding free energy resulting from the Ca^{2+} ion interacting with the residues in either the pEF or the cEF hand for the fully-saturated holo and half-saturated simulations. We used the molecular mechanics/Poisson Boltzmann surface area analysis (MM/PBSA) program (5–8), which is part of the AMBER 14 package (9), to perform calculations on 100 snapshots corresponding to one snapshot per nanosecond sampled with the cpptraj program. The binding free energy, calculated by the MM/PBSA program, is defined as:

$$\begin{aligned} \Delta G_{bind} &= G_{complex} - G_{protein} - G_{ligand} \\ &= \Delta E_{MM} + \Delta G_{PB} + \Delta G_{nonpolar} - T\Delta S \end{aligned} \tag{S1}$$

where ΔE_{MM} is the change in the molecular mechanical energy (computed using the molecular dynamics engine), ΔG_{PB} is the change in the solvation free energy determined with the Poisson-Boltzmann equation, $\Delta G_{nonpolar}$ is the change in the non-polar free energy based on a surface area calculation, and $T\Delta S$ is the temperature of the simulation multiplied by the change in entropy. For comparison against our electrostatic score, we extracted the electrostatic contribution to ΔE_{MM}. Here, only the Ca^{2+} ion, acting as the ligand, and the 12 or 14 residues making up the respective EF hand, acting as the receptor, were included in the calculations. As reported in the main text for our electrostatic score, the holo state's cEF has a significantly more favorable electrostatic interaction energy than the pEF hand. This trend is verified by identical rankings based on MM electrostatic energies (see Fig. S2 and Table S3 in Section 1.3.4). Namely, for the holo case the interaction energy between the Ca^{2+} ion and the

residues in the cEF hand is more favorable by 409.1 kcal/mol than in the pEF hand. These data support that our electrostatic score is reliable and accurately reflects the trends shown in the MM electrostatic energies. However, an advantage of the electrostatic score is that we can qualitatively estimate the strength of electrostatic cases in cases lacking the Ca^{2+} ion (specifically the apo state and vacant pEF hand of the half-saturated state). This advantage permits the estimation of how reordering chelating oxygens in the holo state relative to the apo improves the Ca^{2+} electrostatic interaction energy.

1.3 Results

1.3.1 Region definitions and Ca^{2+} coordination

Table S1: Residue ranges for the S100A1 four alpha-helices.

Configuration	PDB ID	Helix 1	pEF	Helix 2	Helix 3	cEF	Helix 4
Apo	2L0P (10)	3-18	19-32	30-41	51-64	62-73	71-86
Apo	2LLU (11)	3-17	19-32	30-40	51-63	62-73	71-86
Holo	2LP3 (12)	3-20	19-32	30-40	53-61	62-73	71-91

1.3.2 RMSFs indicate the flexibility of various regions of the protein

RMSFs, like the order parameters, are indicators of protein flexibility. In previous work examining Ca^{2+} binding to the EF hand protein troponin C (TnC) (13, 14), we found that root-mean square fluctuations (RMSF) of the Ca^{2+} binding loop backbone carbons were comparable to the amide order parameters. We furthermore noted that one TnC mutant appeared to suppress backbone fluctuations in the apo state, which we argued explained the experimentally reduced Ca^{2+} association rates as minimal reorganization of the binding site was necessary to accommodate the Ca^{2+} ions. As discussed above, measurements of protein flexibility show the stabilizing force of the Ca^{2+} ion on the local and global protein structure. The trends in the RMSFs are expected to mirror those

Table S2: Holo state Ca^{2+}/oxygen coordination distances for experimental and simulated structures.

Coordinate oxygen	EF hand	NMR (PDB ID: 2LP3 (12)) [Å]	Simulated [Å]
S19 O	pEF	2.44 ± 0.04	2.36 ± 0.18
E22 O		2.44 ± 0.03	2.71 ± 1.02
D24 O		2.51 ± 0.04	2.56 ± 0.61
K27 O		2.46 ± 0.05	2.53 ± 0.42
E32 $O_{\epsilon 1}$		2.43 ± 0.19	2.25 ± 0.10
E32 $O_{\epsilon 2}$		2.80 ± 0.29	2.32 ± 0.11
E62 $O_{\delta 1}$	cEF	2.33 ± 0.41	2.49 ± 0.67
N64 $O_{\delta 1}$		2.55 ± 0.04	4.26 ± 2.28
D66 $O_{\delta 1}$		2.83 ± 0.33	2.27 ± 0.16
D66 $O_{\delta 2}$		2.41 ± 0.23	2.77 ± 0.63
E68 O		2.53 ± 0.04	2.31 ± 0.08
E73 $O_{\epsilon 1}$		2.69 ± 0.37	2.35 ± 0.42
E73 $O_{\epsilon 2}$		2.91 ± 0.57	2.36 ± 0.19

of the experimental order parameters in Fig. S1. For example, we expect the pEF and cEF hands in the apo protein to be more flexible than those of the holo protein since they lack the Ca^{2+} ions to orient the protein structure. However, in the linker region, we expect the apo protein to be more stable as indicated by the experimental order parameters (12). As for the half-saturated state, we expect that the protein backbone would have a greater RMSF in the pEF and cEF regions. The Ca^{2+} ion is missing in the pEF hand, so the protein will not orient itself around it. But, we also expect that the pEF hand ion impacts the cEF because experiments indicate that both ions are necessary to obtain the holo state (15). Thus, we expect the pEF hand shape will affect that of the cEF. This hypothesis is reasonable since the pEF and cEF interact in the form of a β-sheet (see Fig. 1) .

Fig. S1 shows the amide nitrogen RMSF per residue averaged over two chains and four MD simulations. In the S100A1 protein, there are peaks in the RMSF values at residues 19-30 and 40-70. The former region corresponds to the pEF hand, residues S19 to E32. Of the three protein states examined here, the holo

protein had the smallest average RMSF over this region, peaking at 1.25 ± 0.47 Å followed by the apo protein at 2.27 ± 0.84 Å and the half-saturated protein at 2.68 ± 0.78 Å. This trend is appropriate because the holo protein is the only case that has a Ca^{2+} ion to coordinate the residues and thus stabilize the protein conformation. The other two cases lack the structural reinforcement provided by the ion. This trend also agrees with the order parameters shown in Fig. 2. According to the calculated values, the half-saturated state is the most flexible followed by the apo state then the holo one. And the experimental values show that the apo state is more flexible than the holo one at the pEF hand (12).

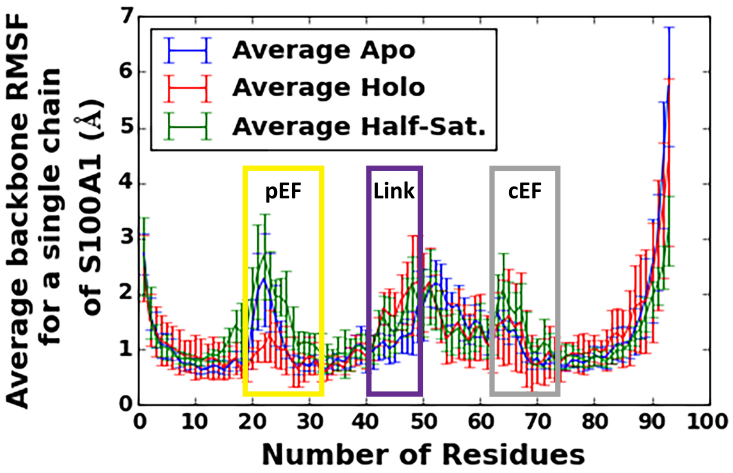

Figure S1: Backbone amide nitrogen RMSF per residue of the apo (blue), holo (red), and half-saturated (green) averaged over the two homo-dimer chains and the four MD runs. The pEF (yellow), linker (purple), and cEF (gray) regions are outlined.

The second region (residues E40 to D70) corresponds to the linker region at residues L41 to D50 and the cEF hand at residues D62 to E73. In the linker region, there is a steady increase in RMSF with increasing residue number. The holo and half-saturated cases consistently have RMSFs greater by 0.5 Å than the apo state, which agrees with the experimental and calculated order parameters that show the apo state is least flexible in this region, but only slightly so. The

opposite trend is observed in the helical region at residues D50 to L61: the RMSF decreases with increasing residue number, and the apo case's RMSF is consistently 0.5 Å greater than the holo and half-saturated cases. For the cEF region, the half-saturated state has the largest RMSF, peaking at 2.07 ± 0.66 Å, followed by the apo state at 1.65 ± 0.29 Å and the holo state at 1.48 ± 0.92 Å. This trend of protein state and corresponding peak maxima matches that of the pEF hand, but unlike the former region, the differences for each protein case are not statistically significant.

1.3.3 Electrostatic scores assuming identical oxygen charges for backbone and side chain oxygens

We also show that the types of interactions with the protein play an important role in determining the strength of the electrostatic scores (Fig. 4B). When all the oxygens are assigned the same charge as the backbone oxygens, then the difference in the electrostatic scores between the pEF and cEF hands decrease significantly. The electrostatic score for the holo cEF hand with the backbone charges is -5.57, which is 1.75 less favorable than that of its counterpart in Fig. 4A. This new score is also much closer to that of the holo pEF hand with the difference being only 0.61 as opposed to 1.46 for the case above. These results suggest that the composition of oxygen atoms play an important role in effecting the binding affinity. Four of the seven oxygen atoms chelating with the Ca^{2+} ion in the pEF hand are backbone oxygens, whereas only one of the coordinating oxygen atoms is a backbone oxygen in the cEF hand. Since the side-chain oxygens have an increased negative charge, they have more favorable electrostatic interactions, and thus, would explain an improved binding affinity.

1.3.4 MM electrostatic energies versus Electrostatic scores

In order to validate out electrostatic score method, we calculated the MM electrostatic energy between the Ca^{2+} ion and the residues in the EF hand. Our results for these trials are shown in Fig. S2 and Table S3. The energetic trends

between the pEF and the cEF hands of the holo state match what was observed above in the electrostatic score calculations. The pEF hand has significantly less favorable MM electrostatic energies than the cEF hand, -168.0 ± 13.0 kcal/mol versus -577.1 ± 25.3 kcal/mol respectively, which agrees with what we determined from the electrostatic score calculations. These results agree with the experiments that show that Ca^{2+} ions have a stronger binding affinity to the cEF hand than the pEF hand (15, 16). The energetic trends for the cEF hand of the half-saturated versus fully saturated holo states are similar for both the MM electrostatic energy and the calculated electrostatic scores. The cEF hands have statistically similar energies for the half-saturated and holo states, -584.0 ± 21.3 kcal/mol versus -577.1 ± 25.3 kcal/mol respectively. This observation further supports the observation of non-cooperativity between the two hands since the absence of the Ca^{2+} ion in the pEF hand does not seem to affect the energetics of Ca^{2+} binding in the cEF hand. These data suggest that the electrostatic scores and MM electrostatic energies are in relative agreement.

1.3.5 β-sheet hydrogen bond between K31 in the pEF hand and G65 in the cEF hand

In Fig. S3, we compare MD simulations of the holo and apo states after 100 ns. It is notable that the shape of the EF hands and the adjoining β-sheet change significantly between the apo and holo states. In the holo state, G65 moves far from its position in the apo state because it is between N64 and D66, both of which coordinate with the Ca^{2+} ion. Thus, when the EF hands reorient themselves around the Ca^{2+} ion, the interaction is broken between K31 and G65 in order to form new interactions.

Table S3: Raw data and calculated average MM electrostatic energy [kcal/mol] (extracted from MM/PBSA calculations) between the Ca^{2+} ion and the residues in the respective EF hands for the half-saturated and fully saturated holo states. The pEF hand and cEF hand consist of residues S19 to E33 and D62 to E73, respectively. The respective standard deviations for the eight cases were calculated by AMBER's MM/PBSA program and are averaged over the course of the simulation.

Case	EF hand	Run	Chain	Average Electrostatic Energy [kcal/mol]
Half-Sat.	cEF	1	A	-602.4 ± 8.2
		1	B	-598.6 ± 10.6
		2	A	-597.0 ± 22.8
		2	B	-598.7 ± 31.7
		3	A	-540.0 ± 13.0
		3	B	-559.8 ± 16.6
		4	A	-579.3 ± 13.4
		4	B	-595.9 ± 8.2
			Mean	**-584.0 ± 21.3**
Holo	cEF	1	A	-594.4 ± 7.1
		1	B	-597.4 ± 9.0
		2	A	-592.4 ± 22.2
		2	B	-601.7 ± 9.7
		3	A	-532.4 ± 16.9
		3	B	-568.1 ± 26.5
		4	A	-540.7 ± 9.6
		4	B	-589.8 ± 7.8
			Mean	**-577.1 ± 25.3**
Holo	pEF	1	A	-163.9 ± 9.6
		1	B	-180.3 ± 22.4
		2	A	-170.0 ± 8.0
		2	B	-181.1 ± 11.0
		3	A	-185.2 ± 24.0
		3	B	-164.8 ± 9.8
		4	A	-150.2 ± 9.6
		4	B	-148.5 ± 8.3
			Mean	**-168.0 ± 13.0**

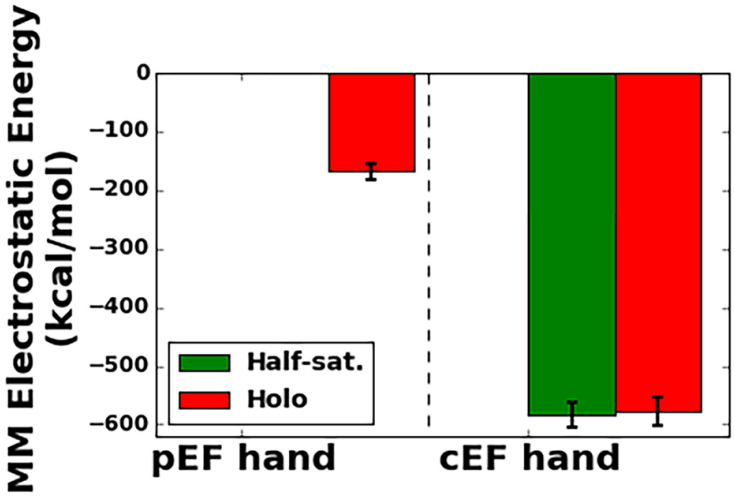

Figure S2: Calculated MM electrostatic energy (extracted from MM/PBSA calculations) between the Ca^{2+} ion and the residues in the respective EF hands for the half-saturated (green) and fully saturated holo (red) states averaged over quadruplicate simulations. The pEF hand and cEF hand consist of residues S19 to E33 and D62 to E73, respectively. Vertical error bars indicate the standard deviation of the eight mean electrostatic scores for two protein chains and the four simulation runs. The trends shown here for the MM electrostatic scores agree with those shown for the electrostatic scores in Fig. 4.

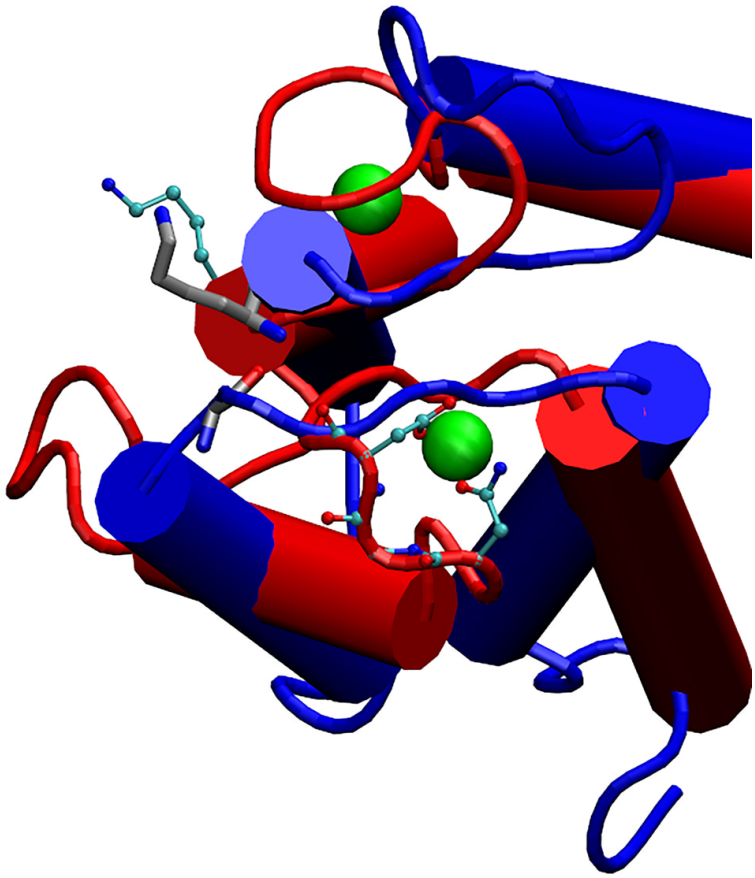

Figure S3: A comparison of the EF hands in chain A of the apo (blue) and the holo (red) forms of the S100A1 protein. K31 and G65 are shown in gray licorice for the apo case, and K31, N64, G65, and D66 are shown in cyan CPK for the holo case. Ca^{2+} ions are green.

1.3.6 Principle component analysis on the extended half-saturated cases

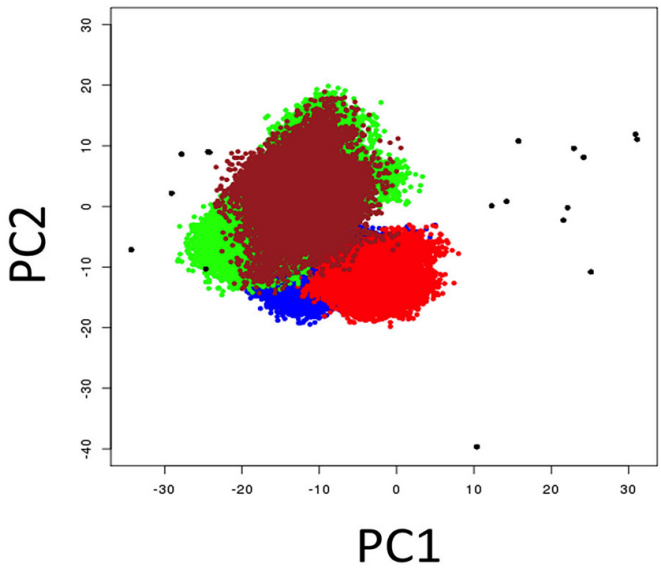

Figure S4: PCA for the four extended simulation runs of the half-saturated states.

Bibliography

1. Miyamoto, S., and P. A. Kollman, 1992. SETTLE: An analytical version of the SHAKE and RATTLE algorithm for rigid water models. *J. Comput. Chem.* 13:952–962. 1.1.1

2. Ryckaert, J. P., G. Ciccotti, and H. J. C. Berendsen, 1977. Numerical integration of cartesian equations of motion of a systerm with constratints: Molecular dynamics of N-alkanes. *J. Comput. Phys.* 23:327–341. 1.1.1

3. Berendsen, H. J. C., J. P. M. Postma, W. F. Vangunsteren, A. Dinola, and J. R. Haak, 1984. Molecular dynamics with coupling to an external bath. *J. Chem. Phys.* 81:3684–3690. 1.1.1

4. Darden, T., D. York, and L. Pedersen, 1993. Particle mesh Ewald: An N.log(N) method for Ewald sums in large systems. *J. Chem. Phys.* 98:10089–10092. 1.1.1

5. Kollman, P. A., I. Massova, C. Reyes, B. Kuhn, S. H. Huo, L. Chong, M. Lee, T. Lee, Y. Duan, W. Wang, O. Donini, P. Cieplak, J. Srinivasan, D. A. Case, and T. E. Cheatham, 2000. Calculating structures and free energies of complex molecules: Combining molecular mechanics and continuum models. *Acc. Chem. Res.* 33:889–897. 1.2

6. Gohlke, H., and D. A. Case, 2004. Converging free energy estimates: MM-PB(GB)SA studies on the protein-protein complex Ras-Raf. *J. Comput. Chem.* 25:238–250.

7. Hou, T., J. Wang, Y. Li, and W. Wang, 2011. Assessing the Performance of the Molecular Mechanics/Poisson Boltzmann Surface Area and Molecular Mechanics/Generalized Born Surface Area Methods. II. The Accuracy of Ranking Poses Generated From Docking. *J. Comput. Chem.* 32:866–877.

8. Miller, I., Bill R., J. McGee, T. Dwight, J. M. Swails, N. Homeyer, H. Gohlke, and A. E. Roitberg, 2012. MMPBSA.py: An Efficient Pro-

gram for End-State Free Energy Calculations. *J. Chem. Theory Comput.* 8:3314–3321. 1.2

9. Case, D., V. Babin, J. Berryman, R. Betz, Q. Cai, D. Cerutti, T. Cheatham III, T. Darden, R. Duke, H. Gohlke, A. Goetz, S. Gusarov, N. Homeyer, P. Janowski, J. Kaus, I. Kolossvary, A. Kovalenko, T. Lee, S. LeGrand, T. Luchko, R. Luo, B. Madej, K. Merz, F. Paesani, D. Roe, A. Roitberg, C. Sagui, R. Salomon-Ferrer, G. Seabra, C. Simmerling, W. Smith, J. Swails, R. Walker, J. Wang, R. Wolf, X. Wu, and P. Kollman, 2014. AMBER 14. 1.2

10. Nowakowski, M., L. Jaremko, M. Jaremko, I. Zhukov, A. Belczyk, A. Bierzyriski, and A. Ejchart, 2011. Solution NMR structure and dynamics of human apo-S100A1 protein. *J. Struct. Biol.* 174:391–399. S1

11. Zivkovic, M. L., M. Zareba-Koziol, L. Zhukova, J. Poznanski, I. Zhukov, and A. Wyslouch-Cieszynska, 2012. Post-translational S-nitrosylation is an endogenous factor fine tuning the properties of human S100A1 protein. *J. Biol. Chem.* 287:40457–40470. S1

12. Nowakowski, M., K. Ruszczynska-Bartnik, M. Budzinska, L. Jaremko, M. Jaremko, K. Zdanowski, A. Bierzynski, and A. Ejchart, 2013. Impact of calcium binding and thionylation of S100A1 protein on its Nuclear Magnetic Resonance-derived structure and backbone dynamics. *Biochemistry* 52:1149–1159. S1, S2, 1.3.2

13. Kekenes-Huskey, P., S. Lindert, and J. McCammon, 2012. Molecular basis of calcium-sensitizing and desensitizing mutations of the human cardiac troponin C regulatory domain: a multi-scale simulation study. *PLoS Comp. Biol.* 8:e1002777–e1002777. 1.3.2

14. Lindert, S., P. Kekenes-Huskey, G. Huber, L. Pierce, and J. McCammon, 2012. Dynamics and calcium association to the N-terminal regulatory domain of human cardiac troponin C: a multiscale computational study. *J. Phys. Chem. B* 116:8449–8459. 1.3.2

15. Goch, G., S. Vdovenko, H. Kozlowska, and A. Bierzynski, 2005. Affinity of S100A1 protein for calcium increases dramatically upon glutathionylation. *FEBS J.* 272:2557–2565. 1.3.2, 1.3.4

16. Wright, N. T., K. M. Varney, K. C. Ellis, J. Markowitz, R. K. Gitti, D. B. Zimmer, and D. J. Weber, 2005. The three-dimensional solution structure of Ca2+-bound S100A1 as determined by NMR spectroscopy. *J. Mol. Biol.* 353:410–426.